Using 4D STEM to Probe Mesoscale Order in Molecular Glass Films Prepared by Physical Vapor Deposition

Debaditya Chatterjee, Shuoyuan Huang, Kaichen Gu, Jianzhu Ju, Junguang Yu, Harald Bock, Lian Yu, M. Ediger, Paul Voyles

Using 4D STEM to Probe Mesoscale Order in Molecular Glass Films Prepared by Physical Vapor Deposition

Debaditya Chatterjee, Shuoyuan Huang, Kaichen Gu, Jianzhu Ju, Junguang Yu, Harald Bock, Lian Yu, M. D. Ediger, and Paul M. Voyles*

ABSTRACT: Physical vapor deposition can be used to prepare highly stable organic glass systems where the molecules show orientational and translational ordering at the nanoscale. We have used low-dose four-dimensional scanning transmission electron microscopy (4D STEM), enabled by a fast direct electron detector, to map columnar order in glassy samples of a discotic mesogen using a 2 nm probe. Both vapor-deposited and liquid-cooled glassy films show domains of similar orientation, but their size varies from tens to hundreds of nanometers, depending on processing. Domain sizes are consistent with surface-diffusion-mediated ordering during film deposition. These results demonstrate the ability of low-dose 4D STEM to characterize a mesoscale structure in a molecular glass system which may be relevant to organic electronics.

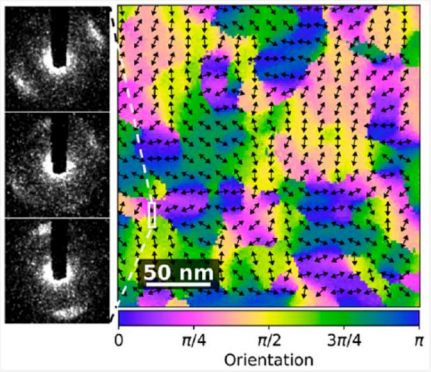

KEYWORDS: *molecular glasses, scanning transmission electron microscopy, physical vapor deposition, nanoscale ordering*

Physical vapor deposition (PVD) can synthesize stable glassy phases of many materials,[1−4] but for organic molecules, PVD can prepare a more unusual material: glasses in which the molecules show overall orientational ordering.[5] This anisotropy in structure causes anisotropy in optical,[6] mechanical,[7] and electronic properties,[8] making the films potentially useful for organic electronics.[9] Discotic mesogens are attractive for applications in organic electronic devices, as they can show columnar ordering via $\pi-\pi$ stacking of molecules, one-dimensional charge mobility,[14] and alignment relative to the substrate that can be tailored for various applications.[8] Phenanthro[1,2,3,4-*ghi*]perylene-1,6,7,12,13,16-hexacarboxylic 6,7,12,13-tetraethyl, 1,16-dimethyl ester ("phenanthroperylene ester", henceforth) is a discotic mesogen designed for applications in organic heterojunction devices. It forms a glassy phase due to the presence of a distorted arene core, which suppresses crystallization while maintaining electronic properties, and it has a relatively low molecular weight, which enables PVD at moderate evaporation temperatures.[15] It forms a hexagonal columnar liquid crystal phase upon cooling from the isotropic liquid phase at 519 K and undergoes a glass transition at 393 K.[16]

Previous research on molecular glass films has shown that ordering during PVD is mediated by the film surface and the surface−vacuum interface during growth[13] and that varying PVD conditions can create various orientation-ordered structures. Increasing the substrate temperature is equivalent to decreasing the deposition rate, a phenomenon called the rate−temperature superposition (RTS),[10−12] and the RTS shift factor depends on the surface mobility. One orientation-ordered structure of phenanthroperylene ester glass involves the discotic molecules orienting edge-on to the surface and organizing into columns via $\pi-\pi$ stacking, as illustrated in Figure 1a. The columns then organize into hexagonal arrays. The X-ray correlation length for the $\pi-\pi$ stacking ($q \approx 1.8$ Å^{-1}) ranges from 1.5 to 3.3 nm (∼4−9 molecules), and the correlation length for the hexagonal packing of the columns ($q \approx 0.4$ Å^{-1}) ranges from 5.1 to 33 nm, which is ∼3−20 molecular diameters, but the in-plane structure is isotropic over macroscopic length scales. X-ray scattering is insensitive to local mesoscale ordering in these samples, especially in-plane. 4D STEM nanodiffraction is sensitive to nano- and mesoscale ordering in glasses,[17−19] and recent developments in fast electron cameras have made possible low-dose experiments on beam-sensitive organic materials.[20−22] However, the low dose has limited the spatial resolution to 5−10 nm and 4D STEM on organic materials has focused on very pronounced nanocrystalline ordering, which produces bright, sharp diffraction features that are easy to detect at a low dose

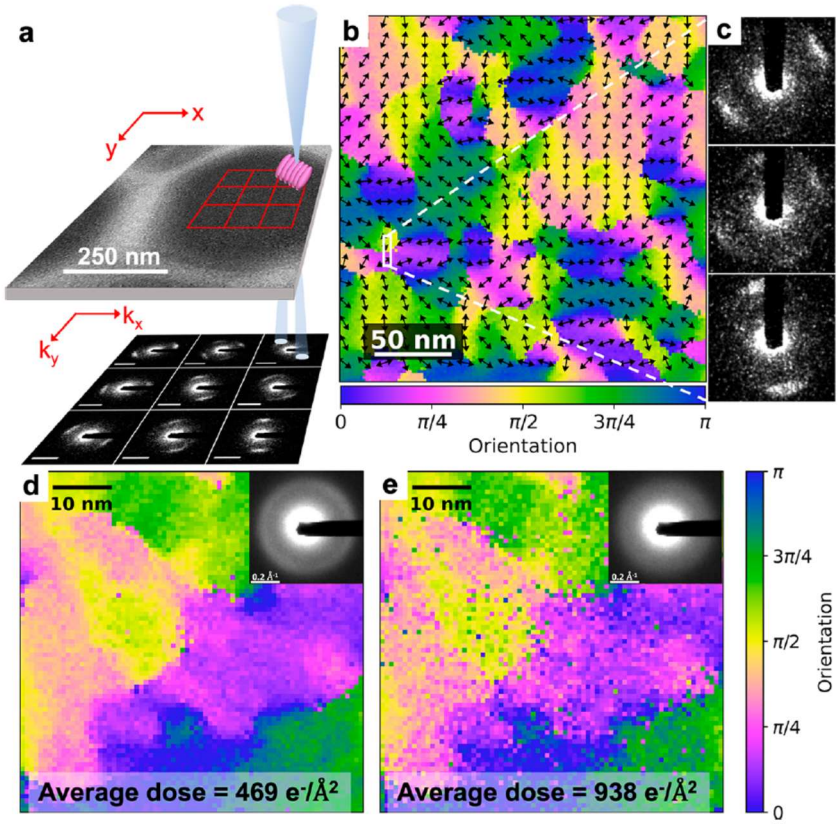

Figure 1. (a) 4D STEM experiment schematic. A diffraction pattern is acquired from each position, as shown with the grid of patterns below the sample. The pink column of disks below the probe is a schematic of the columnar stacking and the diffraction geometry. (b) An orientation map from a 250 nm region on a T_s = 392 K sample constructed from the angle of the diffraction arcs at each position on the sample. Each angle is color-coded from the cyclic color scale shown, which reveals domains having similar orientations within the sample. The arrows overlaid on the map also show the local orientation. (c) Diffraction patterns (spatially averaged and Gaussian filtered to reduce noise from the region in the white rectangle in (b) highlighting variations in the diffraction signal between neighboring domains (top and bottom) and the boundary (middle)) (d, e) Orientation maps at accumulated doses of 469 and 938 $e^-/Å^2$, respectively. Insets: Computed averages of the 4D STEM nanodiffraction patterns acquired with accumulated dose of 469 and 938 $e^-/Å^2$, respectively. The main data sets in this work were acquired at ~117 $e^-/Å^2$ or lower.

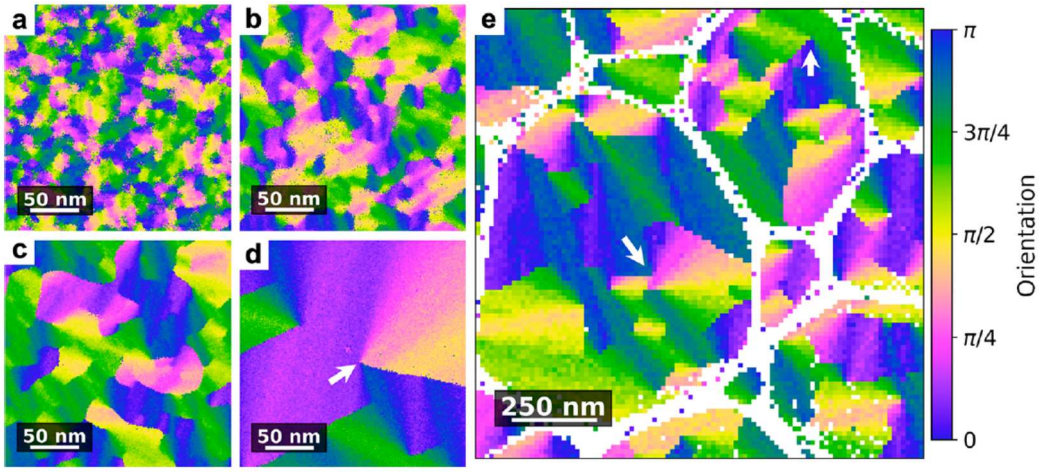

Figure 2. Orientation maps for samples deposited at (a) T_s = 370 K (0.94 T_g), (b) T_s = 380 K (0.97 T_g), and (c) T_s = 392 K (T_g), all with a 252 nm field of view. (d, e) Orientation maps for a liquid-cooled glass with 252 nm and 1.38 μm fields of view, respectively. Arrows point out focal conics. The white regions in (e) are substrate carbon laces.

Here, we use an ultrafast, high-sensitivity direct electron detector[23] to study the mesoscale orientational order in thin films of a phenanthroperylene ester from the scattering signal from the stacking of molecules via π-bonding. We achieve results uninfluenced by beam damage at ~3 nm resolution, which is sufficient to image orientation domains as small as 10 nm, even for the subtle, diffuse scattering features from a glass. The resulting orientation domain maps are consistent with surface diffusion control of the domain size and quantify structural features like domain misorientation that are important for functional properties.

Figure 1a shows the 4D STEM experimental schematic. The diffraction arcs at $k \approx 0.286$ $Å^{-1}$, visible in Figure 1c and Figure S1a, arise from $\pi-\pi$ stacking between the discotic molecules

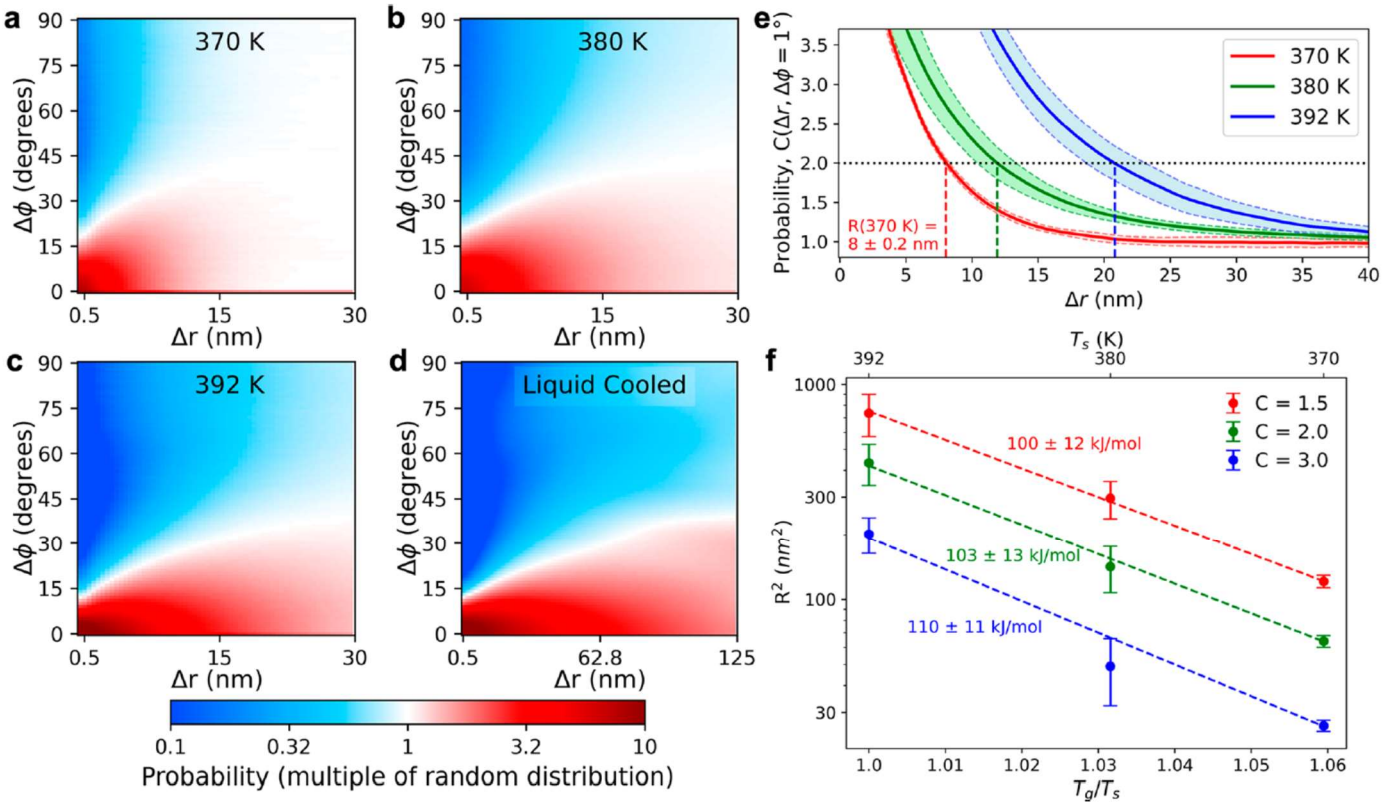

Figure 3. Orientation correlation C as a function of distance (Δr) and misorientation ($\Delta\phi$) for the (a) T_s = 370 K, (b) T_s = 380 K, (c) T_s = 392 K, and (d) liquid-cooled samples. The length scale of orientation in each sample can be visualized through the extent of the red region ($C > 1$). In the PVD samples, the orientations become uncorrelated at $\Delta r < 50$ nm, but for the liquid-cooled sample the orientation persists even at $\Delta r > 100$ nm. (e) Slices through C at $\Delta\phi = 1^\circ$ as a function of Δr, used to determine ordering length, R, for PVD samples. (f) R^2 as a function of T_g/T_s, showing Arrhenius behavior with activation energies near 105 kJ/mol.

with a spacing of ~3.5 Å, which is consistent with previous X-ray scattering investigations[12,16,24] on this material showing a strong peak at $q \approx 1.8$ Å^{-1} ($q = 2\pi k$). The orientation of the arcs therefore reflects the in-plane orientation of the columns of disks. Figure 1b shows a spatial map of the orientation, expressed as an angle between 0 and 180° with respect to the horizontal, for a T_s = 392 K sample, derived by processing many diffraction patterns as described in the Supporting Information. Each angle is assigned a color from the cyclic color scale, and the arrows overlaid on the map also show the local orientation. Domains tens of nanometers across have similar orientations and extend through the 40 nm thickness of the sample. The nanodiffraction data are a 2D projection of the structure through the thickness in the beam direction. Most of the nanodiffraction patterns look like the top and bottom patterns in Figure 1c, with only one set of arcs indicating only one domain through the thickness. The middle pattern in Figure 1c comes from the boundary. Additional structural features like local disorder and out-of-plane columnar orientation can be extracted from the 4D STEM data sets, as discussed in Figure S2.

The phenanthroperylene ester molecules are damaged by exposure to the electron beam.[25,26] The orientation maps in Figure 1d,e acquired at doses of 469 and 938 e$^-$/Å^2, respectively, show domains with similar sizes and shapes, but the map acquired after a higher dose is noisier because damage has reduced the visibility of the diffraction arc features and thus the reliability of the data analysis. The rest of the orientation maps presented here were acquired at ~117 e$^-$/Å^2 or lower; thus, they have minimal impact from beam damage. A further analysis of beam damage on these samples is presented in Figure S3.

Figure 2 shows example orientation maps from samples prepared under different processing conditions. Figure 2a–c from vapor-deposited samples reveal orientation domains that roughly triple in size as the substrate temperature is increased from 370 to 392 K. Figure 2d,e shows orientation maps from a film that was deposited, then heated to close to the liquid-crystal ordering temperature, and then cooled back into a glass. This liquid-cooled glass sample shows much larger domains extending over several hundred nanometers. It also shows typical liquid-crystal defects. Points in the map around which the orientation varies smoothly are focal conics in a planar alignment, a defect in columnar hexagonal liquid crystals and smectic A liquid crystals.[30,31] There have been previous polarized microscopy,[32] AFM,[33] and TEM[34] reports on the structure and length scale of focal conic domains, but this is the first observation at nanometer-scale spatial resolution. Additional orientation maps are shown in Figures S4a–S7a. 4D STEM data from samples deposited at T_s = 335 K and T_s = 355 K (not shown) exhibit a continuous ring in nanodiffraction, not arcs: so either they do not have strong in-plane ordering or the in-plane ordering domain size is small compared to the 40 nm sample thickness.

Figure 3 shows the orientation correlation probability, C, of similar columnar orientations at a distance (Δr) and misorientation ($\Delta\phi$), averaged over the several orientation maps, for the T_s = 370, 380, 392 K and and liquid-cooled samples. C is given by[20]

$$C(\Delta r, \Delta\phi) = \frac{\langle I(r, \phi)I(r + \Delta r, \phi + \Delta\phi)\rangle_{r,\phi}}{\langle I(r, \phi)\rangle^2_{r,\phi}},$$

where $\langle\cdots\rangle_{r,\phi}$ indicates averaging over probe positions and azimuthal angle in nanodiffraction. It is normalized to the probability for a random distribution of columnar orientations; thus, the large value near the origin indicates strong ordering within the orientation domains. We extract an ordering length scale R, related to a domain size, by $C(\Delta r)$ at fixed $\Delta\phi = 1°$, the minimum misorientation calculated, shown in Figure 3e. The solid traces are mean C values from multiple data sets for each sample, and the shaded regions are uncertainties estimated as the standard deviation of the mean (see Figures S4b–S7b). R is defined as the Δr value at a fixed value of C (>1) for each sample. Figure 3e illustrates this process for $C(\Delta r,\Delta\phi{=}1°) = 2$, which results in $R = 8.0 \pm 0.2$, 11.9 ± 1.4, and 20.8 ± 2.2 nm for the 370, 380, and 392 K samples, respectively. Uncertainties in R are estimated from the uncertainty in C. Figure 3f shows that the ordering lengths follow an Arrhenius relationship with an activation energy near 105 kJ/mol, independent of the choice of C used to determine R.

The orientation domain size of the as-deposited films is controlled by surface diffusion of the molecular orientation during growth. Surface diffusivity for many glasses is orders of magnitude faster than bulk diffusivity at temperatures near T_g, like the substrate temperatures used here.[27] High surface diffusivity means that newly deposited molecules can sample many configurations during the surface residence time, t_{res}, before they are buried by more deposition. Sampling many configurations allows energetically favorable states to be found.[1] Once the molecules are buried, they can only access slow bulk dynamics; thus, the surface configuration of each layer is frozen in. Thus, annealing a bulk sample does not show ordering similar to that of depositing a film at the same temperature. The film surface is also important because the film–vacuum interface creates a preferred molecular orientation,[13] which plays a larger role in determining the final molecular orientations and the domain sizes than the substrate–film interface.[5]

The physical picture of anisotropic film growth dominated by surface diffusion is as follows: A layer of molecules is deposited. They reorient fast enough that most of the molecules are aligned with the disks edge-on to the substrate (rather than parallel) by the energy of the film surface–vacuum interface. The disks coalesce to form columns, but the in-plane orientation of the columns is not controlled by the surface–vacuum interface. Domains of similar in-plane column orientation form, and the domain boundaries can shift via changes in the orientation of the disks at the boundary. The surface layer is slowly buried by more deposition, freezing its molecules in place because bulk diffusivity is low. As a result, the domain size is controlled by the surface diffusivity that controls molecular orientation. The domains extend through the thickness of the film because the columns in the surface layer align themselves with the columns in the layers below them to form domains. Even in samples where the extent of in-plane orientation creates domains smaller than 40 nm, the orientation propagates through the thickness of the film due to a templating effect by the lower deposited layers. However, at a low enough temperature, the domain size is small enough that columnar growth is not sustained through the entire film thickness.

This picture is consistent with both the order of magnitude of the domain size and the temperature dependence of the domain size. We can estimate the absolute domain size from the surface diffusion length for molecular orientation during deposition of a monolayer as $R \approx 2\sqrt{D_s(T_s)t_{res}}$. R is the domain size, and D_s is the surface diffusivity. Based on previous work by Bishop et al.[10,12] measuring the birefringence as a function of deposition rate at 392 K, we estimate the relaxation time for molecular orientation at the surface at 392 K to be $\tau \approx$ 2.4 ms. The surface diffusivity from the Debye–Stokes–Einstein equation,[28,29] $D_s = 2r^2/9\tau$, is 50 nm^2/s for a molecular radius, r, of 0.75 nm for phenanthroperylene. At a deposition rate of 0.025 nm/s, t_{res} is ~60 s, the time required to deposit a 1.5 nm thick monolayer (one molecular diameter). These quantities predict $R \approx 100$ nm at 392 K, which is in reasonable agreement with the data in Figure 3e ($R = 27$ nm at 392 K, using $C = 1.5$, for example). The activation energy for D_s is 110 kJ/mol, measured from orientational order in X-ray scattering experiments on PVD samples.[12] $R^2 \propto D_s$ in this model; thus Figure 3f shows R^2 vs $1/T_s$, leading to activation energies of 100–110 kJ/mol for various C, all in in excellent agreement with the activation energy for D_s. The agreement of both absolute diffusivity and temperature dependence is strong evidence that surface diffusion during PVD is responsible for the growth of ordered columnar domains.

The ordering length in the 4D STEM orientation maps (tens to hundreds of nanometers) is much larger than the scattering correlation length (2–5 nm) determined from the inverse peak width in either TEM diffraction (Figure S8) or X-ray scattering (previous studies), showing the added value of the direct determination of the mesoscale structure by 4D STEM. The correlation length depends on fluctuations in both the π–π separation between disks and their orientation. The orientation map domain size depends on the orientation of the π–π separations but is less sensitive to variability in the distance. The larger-scale persistence of domain orientation is likely to be important for charge transport;[8] thus, access to this mesoscale information is critical.

Misorientation across domain boundaries also plays a role in transport.[8] Figure 4 shows the distribution of domain misorientations, defined as a difference in local orientation across a domain boundary, determined from the orientation maps. Low misorientation angles are favored for all samples. The distributions shift toward lower misorientations and become narrower for the higher substrate temperature film and the liquid-cooled glass sample. The peaks are at 15, 11, 9, and 7° for T_s = 370 K, T_s = 380 K, and T_s = 392 K and liquid-cooled glass samples, respectively, and the respective half-widths at half-maximum are 17, 9, 6, and 3° for the same samples. Experiments at a lower dose (60 e$^-$/Å^2) show distributions with similar widths; thus, the contribution of beam damage to Figure 4 is small. The preference for low misorientation boundaries and the curved nature of the domain boundaries in PVD samples suggest that low misorientation boundaries have lower interfacial energy than higher misorientation boundaries. In general, films with larger domains and lower misorientation boundaries should have a higher charge mobility; thus, PVD may provide access to higher mobility films than can be achieved via bulk processing at the same temperature.

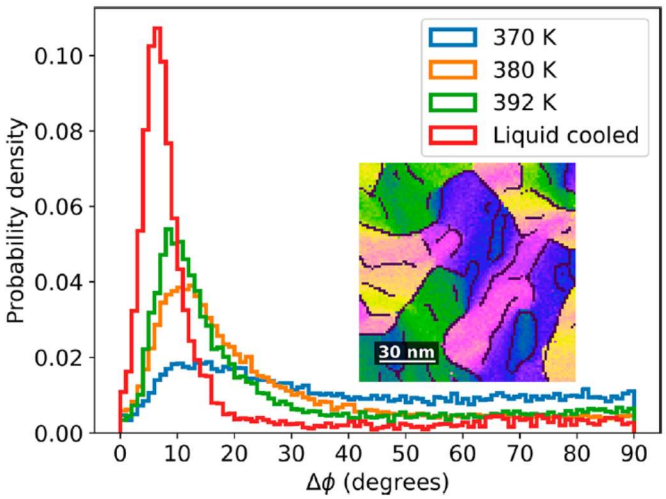

Figure 4. Boundary misorientation distributions for T_s = 370, 380, 392 K and liquid-cooled glass samples. Inset: orientation map from a 392 K sample showing domain boundaries determined using the Canny edge detection algorithm (see the Supporting Information).

These results demonstrate the value of 4D STEM with a high-speed camera like the Direct Electron Celeritas, which enables a high degree of control over electron dose and spatial sampling.[35] The Celeritas runs at up to ∼86000 fps and has high gain and low noise for single-electron sensitivity.[23] With a 0.6 pA probe, an exposure time of 8 ms (125 fps) is sufficient to record enough signal, depositing a dose of ∼100 $e^-/Å^2$, which allows a small probe step (∼2 nm) for improved spatial resolution and lets us map larger regions on the sample without significant sample drift during the acquisition time. Other experiments[20] have used probe steps larger than the probe diameter to minimize dose and beam damage, which we can also do for large domains (see Figure 2e).

Finally, are these materials really glasses? They exhibit very strong structural order in several ways, with a preferred overall orientation for the molecules in one direction and local preferred orientations in another. The nanodiffraction could come from a textured polycrystalline material, as could the orientation domain maps. The liquid-cooled sample even has well-defined line defects! It is helpful to make a distinction between glasses and amorphous materials. Calling a material a glass is a statement about its kinetics: does it exhibit a glass transition on heating and cooling? Calling a material amorphous is a statement about structure: does it lack long-range order, especially in wide-area diffraction? These phenanthroperylene ester films do exhibit a glass transition in calorimetry;[16] thus, they are glasses despite their structural order. Questions like "how structurally ordered can a material be and still be a glass?" and "how do these materials change their structural order through the glass transition?" are interesting topics for future research.

In summary, low-dose, high-speed 4D STEM experiments show that vapor-deposited glassy thin films of a discotic liquid-crystal molecule form domains with a local preferred in-plane orientation for the $\pi-\pi$ stacking direction of the disks. The average domain size increases with substrate temperature, and the average misorientation across domain boundaries decreases. The domain size is controlled by the surface diffusivity for reorientation of the disks: the film−vacuum interface promotes an edge-on orientation for the disks, which stack into columns, and the in-plane orientation of the columns is determined by diffusion of the domain boundaries by reorientation of disks. Large in-plane domains and low domain misorientations are likely to favor high charge mobility; thus, the capability to control the structural order of such materials by direct deposition, without high-temperature annealing, may be beneficial for organic electronics. This study sets the stage for further investigations into fundamental ordering processes in organic systems.

AUTHOR INFORMATION

Corresponding Author

Paul M. Voyles − *Department of Materials Science and Engineering, University of Wisconsin—Madison, Madison, Wisconsin 53706, United States;* orcid.org/0000-0001-9438-4284; Email: paul.voyles@wisc.edu

Authors

Debaditya Chatterjee − *Department of Materials Science and Engineering, University of Wisconsin—Madison, Madison, Wisconsin 53706, United States; Applied Materials Inc., Santa Clara, California 95054, United States;* orcid.org/0000-0001-6010-5152

Shuoyuan Huang − *Department of Materials Science and Engineering, University of Wisconsin—Madison, Madison, Wisconsin 53706, United States*

Kaichen Gu − *Department of Chemistry, University of Wisconsin—Madison, Madison, Wisconsin 53706, United States;* Present Address: Exponent, New Territories, Hong Kong SAR, People's Republic of China

Jianzhu Ju − *Department of Chemistry, University of Wisconsin—Madison, Madison, Wisconsin 53706, United States*

Junguang Yu − *School of Pharmacy, University of Wisconsin—Madison, Madison, Wisconsin 53705, United States;* orcid.org/0000-0001-6458-8307

Harald Bock − *Centre de Recherche Paul Pascal-CNRS & Université de Bordeaux, 33600 Pessac, France*

Lian Yu − *School of Pharmacy, University of Wisconsin—Madison, Madison, Wisconsin 53705, United States;* orcid.org/0000-0002-4253-5658

M. D. Ediger − *Department of Chemistry, University of Wisconsin—Madison, Madison, Wisconsin 53706, United States;* orcid.org/0000-0003-4715-8473

Author Contributions

P.M.V. and M.D.E. conceived the study. D.C. did the 4D STEM experiments and analyzed the data. S.H. and D.C. wrote the analysis software. K.G. and J.J. grew the films. J.Y., D.C., and L.Y. processed the films to obtain the liquid-cooled sample. H.B. synthesized the phenanthroperylene molecules.

M.D.E., L.Y., and D.C. developed the diffusion growth model. D.C. and P.M.V. wrote the manuscript. All authors helped develop the results and conclusions and edited the manuscript.

Notes

The authors declare no competing financial interest.

■ ACKNOWLEDGMENTS

Primary funding for the work was provided by the Wisconsin MRSEC (NSF DMR-1720415). The authors gratefully acknowledge Carter Francis (University of Wisconsin—Madison) for developing the Seq-IO library and contributing to HyperSpy and PyXem and for helpful discussions. The authors also thank Colin Ophus (National Center for Electron Microscopy, Lawrence Berkeley National Laboratory, Berkeley, CA, USA) for helpful discussions and help with orientation correlation analysis using py4DSTEM.

■ REFERENCES

(1) Swallen, S. F.; Kearns, K. L.; Mapes, M. K.; Kim, Y. S.; McMahon, R. J.; Ediger, M. D.; Wu, T.; Yu, L.; Satija, S. Organic Glasses with Exceptional Thermodynamic and Kinetic Stability. *Science (80-.)* **2007**, *315* (5810), 353−356.

(2) Rodriguez-Tinoco, C.; Gonzalez-Silveira, M.; Ramos, M. A.; Rodriguez-Viejo, J. Ultrastable Glasses: New Perspectives for an Old Problem. *Rivista del Nuovo Cimento.* **2022**, *45*, 325−406.

(3) Muley, S. V.; Cao, C.; Chatterjee, D.; Francis, C.; Lu, F. P.; Ediger, M. D.; Perepezko, J. H.; Voyles, P. M. Varying Kinetic Stability, Icosahedral Ordering, and Mechanical Properties of a Model Zr-Cu-Al Metallic Glass by Sputtering. *Phys. Rev. Mater.* **2021**, *5* (3), No. 033602.

(4) Zhang, K.; Li, Y.; Huang, Q.; Wang, B.; Zheng, X.; Ren, Y.; Yang, W. Ultrastable Amorphous Sb 2 Se 3 Film. *J. Phys. Chem. B* **2017**, *121* (34), 8188−8194.

(5) Bagchi, K.; Ediger, M. D. Controlling Structure and Properties of Vapor-Deposited Glasses of Organic Semiconductors: Recent Advances and Challenges. *J. Phys. Chem. Lett.* **2020**, *11* (17), 6935−6945.

(6) Philp Chen, H.-M.; Ou, J. J.; Chen, S. H. Glassy Liquid Crystals as Self-Organized Films for Robust Optoelectronic Devices. *Nanoscience with Liquid Crystals* **2014**, 179−208.

(7) Cang, Y.; Wang, Z.; Bishop, C.; Yu, L.; Ediger, M. D.; Fytas, G. Extreme Elasticity Anisotropy in Molecular Glasses. *Adv. Funct. Mater.* **2020**, *30* (23), 2001481.

(8) Eccher, J.; Zajaczkowski, W.; Faria, G. C.; Bock, H.; von Seggern, H.; Pisula, W.; Bechtold, I. H. Thermal Evaporation versus Spin-Coating: Electrical Performance in Columnar Liquid Crystal OLEDs. *ACS Appl. Mater. Interfaces* **2015**, *7* (30), 16374−16381.

(9) Gujral, A.; Yu, L.; Ediger, M. D. Anisotropic Organic Glasses. *Curr. Opin. Solid State Mater. Sci.* **2018**, *22* (2), 49−57.

(10) Bishop, C.; Gujral, A.; Toney, M. F.; Yu, L.; Ediger, M. D. Vapor-Deposited Glass Structure Determined by Deposition Rate−Substrate Temperature Superposition Principle. *J. Phys. Chem. Lett.* **2019**, *10* (13), 3536−3542.

(11) Bishop, C.; Li, Y.; Toney, M. F.; Yu, L.; Ediger, M. D. Molecular Orientation for Vapor-Deposited Organic Glasses Follows Rate-Temperature Superposition: The Case of Posaconazole. *J. Phys. Chem. B* **2020**, *124* (12), 2505−2513.

(12) Bishop, C.; Chen, Z.; Toney, M. F.; Bock, H.; Yu, L.; Ediger, M. D. Using Deposition Rate and Substrate Temperature to Manipulate Liquid Crystal-Like Order in a Vapor-Deposited Hexagonal Columnar Glass. *J. Phys. Chem. B* **2021**, *125* (10), 2761−2770.

(13) Jerome, B. Surface Effects and Anchoring in Liquid Crystals. *Rep. Prog. Phys.* **1991**, *54* (3), 391−451.

(14) Termine, R.; Golemme, A. Charge Mobility in Discotic Liquid Crystals. *Int. J. Mol. Sci.* **2021**, *22* (2), 877.

(15) Kelber, J.; Achard, M.-F.; Durola, F.; Bock, H. Distorted Arene Core Allows Room-Temperature Columnar Liquid-Crystal Glass with Minimal Side Chains. *Angew. Chemie Int. Ed.* **2012**, *51* (21), 5200−5203.

(16) Chen, Z.; Bishop, C.; Thoms, E.; Bock, H.; Ediger, M. D.; Richert, R.; Yu, L. Controlling the Columnar Order in a Discotic Liquid Crystal by Kinetic Arrest of Disc Tumbling. *Chem. Mater.* **2021**, *33* (12), 4757−4764.

(17) Voyles, P.; Hwang, J. Fluctuation Electron Microscopy. In *Characterization of Materials*; Wiley: 2012. DOI: 10.1002/0471266965.com138.

(18) Huang, S.; Francis, C.; Ketkaew, J.; Schroers, J.; Voyles, P. M. Correlation Symmetry Analysis of Electron Nanodiffraction from Amorphous Materials. *Ultramicroscopy* **2022**, *232*, No. 113405.

(19) Yang, Y.; Zhou, J.; Zhu, F.; Yuan, Y.; Chang, D. J.; Kim, D. S.; Pham, M.; Rana, A.; Tian, X.; Yao, Y.; Osher, S. J.; Schmid, A. K.; Hu, L.; Ercius, P.; Miao, J. Determining the Three-Dimensional Atomic Structure of an Amorphous Solid. *Nature* **2021**, *592* (7852), 60−64.

(20) Panova, O.; Ophus, C.; Takacs, C. J.; Bustillo, K. C.; Balhorn, L.; Salleo, A.; Balsara, N.; Minor, A. M. Diffraction Imaging of Nanocrystalline Structures in Organic Semiconductor Molecular Thin Films. *Nat. Mater.* **2019**, *18* (8), 860−865.

(21) Bustillo, K. C.; Zeltmann, S. E.; Chen, M.; Donohue, J.; Ciston, J.; Ophus, C.; Minor, A. M. 4D-STEM of Beam-Sensitive Materials. *Acc. Chem. Res.* **2021**, *54* (11), 2543.

(22) Wu, M.; Harreiß, C.; Ophus, C.; Johnson, M.; Fink, R. H.; Spiecker, E. Seeing Structural Evolution of Organic Molecular Nano-Crystallites Using 4D Scanning Confocal Electron Diffraction (4D-SCED). *Nat. Commun.* **2022**, *13* (1), 2911.

(23) Chatterjee, D.; Wei, J.; Kvit, A.; Bammes, B.; Levin, B.; Bilhorn, R.; Voyles, P. An Ultrafast Direct Electron Camera for 4D STEM. *Microsc. Microanal.* **2021**, *27* (S1), 1004−1006.

(24) Gujral, A.; Gómez, J.; Ruan, S.; Toney, M. F.; Bock, H.; Yu, L.; Ediger, M. D. Vapor-Deposited Glasses with Long-Range Columnar Liquid Crystalline Order. *Chem. Mater.* **2017**, *29* (21), 9110.

(25) Egerton, R. F. Radiation Damage to Organic and Inorganic Specimens in the TEM. *Micron* **2019**, *119*, 72−87.

(26) Egerton, R. F. Mechanisms of Radiation Damage in Beam-Sensitive Specimens, for TEM Accelerating Voltages between 10 and 300 KV. *Microsc. Res. Tech.* 2012, *75* (11). DOI: 10.1002/jemt.22099.

(27) Li, Y.; Zhang, W.; Bishop, C.; Huang, C.; Ediger, M. D.; Yu, L. Surface Diffusion in Glasses of Rod-like Molecules Posaconazole and Itraconazole: Effect of Interfacial Molecular Alignment and Bulk Penetration. *Soft Matter* **2020**, *16* (21), 5062−5070.

(28) Li, D. D.; Greenfield, M. L. Viscosity, Relaxation Time, and Dynamics within a Model Asphalt of Larger Molecules. *J. Chem. Phys.* **2014**, *140* (3), 034507.

(29) Dehaoui, A.; Issenmann, B.; Caupin, F. Viscosity of Deeply Supercooled Water and Its Coupling to Molecular Diffusion. *Proc. Natl. Acad. Sci.* **2015**, *112* (39), 12020−12025.

(30) Fournier, J. B.; Durand, G. Focal Conic Faceting in Smectic-A Liquid Crystals. *J. Phys. II* **1991**, *1* (7), 845.

(31) Kléman, M.; Lavrentovich, O. D. Grain Boundaries and the Law of Corresponding Cones in Smectics. *Eur. Phys. J. E* **2000**, *2* (1), 47.

(32) Bramble, J. P.; Evans, S. D.; Henderson, J. R.; Atherton, T. J.; Smith, N. J. Observations of Focal Conic Domains in Smectic Liquid Crystals Aligned on Patterned Self-assembled Monolayers. *Liq. Cryst.* **2007**, *34* (10), 1137−1143.

(33) Sinitsyna, O. V.; Bobrovsky, A. Y.; Meshkov, G. B.; Yaminsky, I. V.; Shibaev, V. P. Direct Observation of Changes in Focal Conic Domains of Cholesteric Films Induced by Ultraviolet Irradiation. *J. Phys. Chem. B* **2017**, *121* (21), 5407−5412.

(34) Agez, G.; Bitar, R.; Mitov, M. Color Selectivity Lent to a Cholesteric Liquid Crystal by Monitoring Interface-Induced Deformations. *Soft Matter* **2011**, *7* (6), 2841.

(35) Huang, S.; Francis, C.; Sunderland, J.; Jambur, V.; Szlufarska, I.; Voyles, P. M. Large Area, High Resolution Mapping of Approximate Rotational Symmetries in a Pd77.5Cu6Si16.5 Metallic Glass Thin Film. *Ultramicroscopy* **2022**, *241*, No. 113612.